Frontiers of Physics
https://doi.org/10.1007/s11467-019-0898-z
Front. Phys.
14(2), 22601 (2019)

RESEARCH ARTICLE

Optomechanical properties of a degenerate nonperiodic cavity chain

Miao-Miao Zhao[1], Zhuo Qian[1], Bang-Pin Hou[1,*], Yong Liu[2,†], Yong-Hong Zhao[1,‡]

[1] *College of Physics and Electronic Engineering, Center for Computational Sciences, Sichuan Normal University, Chengdu 610068, China*
[2] *State Key Laboratory of Metastable Materials Science and Technology & Key Laboratory for Microstructural Material Physics of Hebei Province, School of Science, Yanshan University, Qinhuangdao 066004, China*
*Corresponding authors. E-mail: * bphou@sicnu.edu.cn, † yongliu@ysu.edu.cn, ‡ yhzhao.cd@gmail.com*
Received January 31, 2019; accepted March 20, 2019

The absorption of single-cavity and double-cavity optomechanical systems and periodic optomechanical lattices has previously been investigated extensively. In this paper, we present the absorption of a nonperiodic cavity chain, where the absorption value on the resonance point shows switchable dips or peaks, according to whether the optomechanical interaction is at an odd or even-numbered position in the chain. Meanwhile, the value of absorption due to the optomechanical interaction varies with the number of the bare cavities. The calculated results may have some novel applications, such as detecting the position of the movable mirror in a long cavity chain, which would be useful in quantum information processing based on optomechanical systems.

Keywords optomechanics, optomechanically induced transparency (OMIT)

1 Introduction

An optomechanical system (OMS) is usually an optical cavity, inside which there is either a movable mirror together with a fixed one [1, 2] or a micromechanical membrane [3]. The movable mirror or membrane is then coupled to the cavity field by the radiation pressure [4]. OMSs have attracted much attention because of their various potential applications, such as cooling mechanical resonators to their quantum ground states [5–8], producing quantum nonlinearities in quantum processing [9–11], optomechanical sensing with on-chip microcavities [12], and achieving stationary entanglement between two macroscopic oscillators and two cavity fields [13–15]. It has also been shown that OMSs can be used to generate macroscopic quantum superposition [16] and slow down light [17, 18].

Although most attention has been paid to single-cavity OMSs, it is also very important for practical application that OMSs can be generalized by integrating more optical or mechanical modes, such applications include quantum information processing, quantum computing [19–21], all-optical bit storage [22], and high precision measurements [23, 24]. For example, in a double-cavity OMS, destructive interference can create a transparency window in the probe absorption and a group delay controlled by the power of the pump beams [25]. The width and height of the electromagnetically induced absorption peak within the transparency window of a double-cavity OMS can be explained in terms of three coupled oscillators with different relaxation parameters [26]. In addition, strongly tunnel-coupled hybridized OMSs exhibit tunable interference induced by the optomechanical interaction [27].

Interference between the phononic and photonic paths has also been presented recently [28]. It has also been confirmed experimentally that two nearly degenerate mechanical resonators, coupled to a single optical cavity, can be hybridized into a bright mode with strong optomechanical interations and a dark mode with almost no optomechanical interactions [29]. This hybridization is useful for transferring energy between mechanical modes. Moreover, the transparency in double quadratically coupled OMSs is theoretically shown to be tuned by the intensity difference between two coupling fields [30].

Recently, much attention has also been paid to optomechanical lattices, which comprise periodically arranged optomechanical cavities. An optical cavity with a periodic of membranes therein can exhibit long-range photonic coherence and a dynamical phase transition [31]. Well known in basic OMSs, optomechanically induced transparency (OMIT) has also been generalized to strongly driven optomechanical lattices [32]. In addition to photons, the quantum state can also be transferred in an optomechanical lattice, with such an ability being at the heart of quantum information processing [33]. Moreover, light pulses can be slowed down and stopped by the band structure of polaritons owing to the interaction between photons and the collective excitation of mechanical resonators [34].

Although OMSs with single, double or periodic cavities have been studied extensively, there has been scarce investigation of the absorption and transparency properties in nonperiodic OMS chain because of the associated

calculations. Herein, we use the newly developed package OMPY (OptoMechanics by PYthon) to investigate the optomechanical properties of a nonperiodic cavity chain [35]. This paper is organized as follows. In Section 2, we model an n-cavity chain and present the dynamical equations of a chain with six cavities. In Section 3, we show the absorption of this six-cavity chain, which can be generalized naturally to a chain with arbitrarily many cavities using OMPY. In Section 4, we generalize the calculation to an infinite chain, wherein we use bare cavities to modulate the OMS absorption. Finally, we summarize our calculations in Section 5.

2 Model and dynamical equations

The OMS considered herein is shown in Fig. 1, where n cavities are coupled with the tunneling interaction $J_{l,l+1}$ ($l = 1, 2, \cdots, n-1$), which is proportional to the transmittance of the two fixed mirrors of each cavity. Each cavity is driven by a control field of amplitude ε_{ci} and frequency ω_{ci}. In order to detect the absorption properties of the OMS, a weak field of amplitude ε_p and frequency ω_p, is usually used to probe the first cavity. In the quadratically coupled situation, the movable mirror is usually located at the antinode of the cavity mode. The cavity frequency can then be approximated using the second order of the displacement $\hat{q}_i$ of the movable mirror, namely, $\omega_i(\hat{q}_i) \sim \omega_{i0} + g_i\hat{q}_i^2$, where ω_{i0} is the resonance frequency of cavity i when the displacement of the movable mirror is zero and g_i is the quadratic coupling constant [3, 17].

Therefore, in the frame rotating at the frequency ω_{ci},

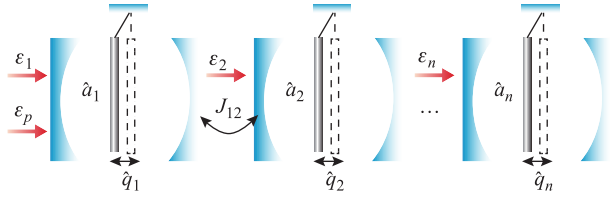

Fig. 1 Schematic diagram of quadratic coupled optomechanical cavity chain. The ith movable mirror is located at the middle position of the ith cavity which is driven by a strong control field ($\varepsilon_i, i = 1, 2, \cdots, n$). Additionally, the first cavity is probed by a weak field (ε_p).

the Hamiltonian of the quadratically coupled optomechanical cavity chain, shown in Fig. 1, can be expressed as follows:

$$\begin{aligned}\hat{H}=&\sum_{i=1}^{n}\hbar\Delta_{ci}\hat{a}_i^+\hat{a}_i+\sum_{i=1}^{n}\left(\frac{\hat{p}_i^2}{2m_i}+\frac{m_i\omega_{mi}^2\hat{q}_i^2}{2}\right)\\&+\sum_{i=1}^{n}\hbar g_i\hat{a}_i^+\hat{a}_i\hat{q}_i^2+\sum_{i=1}^{n}\mathrm{i}\hbar\sqrt{\eta_c\kappa_i}\varepsilon_{ci}(\hat{a}_i^+-\hat{a}_i)\\&+\sum_{l=1}^{n-1}\hbar J_{l,l+1}(\hat{a}_l^+\hat{a}_{l+1}\mathrm{e}^{\mathrm{i}(\omega_{cl}-\omega_{cl+1})t}+\hat{a}_l\hat{a}_{l+1}^+\mathrm{e}^{-\mathrm{i}(\omega_{cl}-\omega_{cl+1})t})\\&+\mathrm{i}\hbar\sqrt{\eta_c\kappa_1}\varepsilon_p(\hat{a}_1^+\mathrm{e}^{-\mathrm{i}\delta t}-\hat{a}_1\mathrm{e}^{\mathrm{i}\delta t}),\end{aligned}\tag{1}$$

in which $\Delta_{ci} = \omega_{i0} - \omega_{ci}$ ($i = 1, 2, \cdots, n$) denotes the detuning between the cavity field and its corresponding coupling field, and $\delta = \omega_p - \omega_{ci}$ is the detuning between the first coupling field and the probe field. $\hat{p}_i$ and ω_{mi} are the momentum operator and angular frequency of the ith movable mirror, while $\hat{a}_i$ and $\hat{a}_i^+$ denote the annihilation and creation operator of the ith cavity mode, respectively. In Eq. (1), the first term denotes the free energies of the n optical cavities, and the second term denotes free energies of the movable mirrors. The third term denotes the quadratic coupling between the mirror and the optical mode, the quadratic coefficient is given by $g_i = \frac{8\pi^2 c}{\lambda_i^2 L_i}\sqrt{\frac{R}{1-R}}$ ($i = 1, 2, \cdots, n$), where c is the speed of light in vacuum, and λ_i is the wavelength of the coupling field. The fifth term denotes the tunnel coupling of strength $J_{l,l+1}$ ($l = 1, 2, \cdots, n-1$) between two adjacent cavities. The fourth term denotes the application of a control field to the n optomechanical cavities, and the final term denotes the weak probe field adding on the first cavity. The amplitudes of the control fields and the probe field have been normalized to the photon flux inputting into the cavities and are defined as $\varepsilon_{ci} = \sqrt{P_{ci}/(\hbar\omega_{ci})}$ and $\varepsilon_p = \sqrt{P_p/(\hbar\omega_p)}$, respectively, where P_{ci} is the power of the control field and P_p is the power of probe field. Moreover, the coupling parameter $\eta_c \equiv \kappa_{ex}/\kappa$, where κ and κ_{ex} denote the cavity decay rate and the external loss rate, can be adjusted continuously but is fixed herein as 1/2. In order to study the system's dynamical equations, we set $n = 6$. In this case, after taking the corresponding noise and damping terms into consideration and considering the factorization assumption, the Heisenberg–Langevin equations of this system can be written as

$$\frac{\mathrm{d}\langle\hat{a}_1\rangle}{\mathrm{d}t} = -\mathrm{i}\Delta_{c1}\langle\hat{a}_1\rangle - \mathrm{i}g_1\langle\hat{q}_1^2\rangle\langle\hat{a}_1\rangle - \mathrm{i}J_{1,2}\langle\hat{a}_2\rangle + \varepsilon_{c1}\sqrt{\eta_c\kappa_1} + \varepsilon_p\sqrt{\eta_c\kappa_1}\mathrm{e}^{-\mathrm{i}\delta t} - \frac{\kappa_1}{2}\langle\hat{a}_1\rangle,\tag{2a}$$

$$\frac{\mathrm{d}\langle\hat{a}_i\rangle}{\mathrm{d}t} = -\mathrm{i}\Delta_{ci}\langle\hat{a}_i\rangle - \mathrm{i}g_i\langle\hat{q}_i^2\rangle\langle\hat{a}_i\rangle - \mathrm{i}J_{i-1,i}\langle\hat{a}_{i-1}\rangle - \mathrm{i}J_{i,i+1}\langle\hat{a}_{i+1}\rangle + \varepsilon_{ci}\sqrt{\eta_c\kappa_i} - \frac{\kappa_i}{2}\langle\hat{a}_i\rangle,\quad i = 2, 3, 4, 5,\tag{2b}$$

$$\frac{\mathrm{d}\langle\hat{a}_6\rangle}{\mathrm{d}t} = -\mathrm{i}\Delta_{c6}\langle\hat{a}_6\rangle - \mathrm{i}g_6\langle\hat{q}_6^2\rangle\langle\hat{a}_6\rangle - \mathrm{i}J_{5,6}\langle\hat{a}_5\rangle + \varepsilon_{c6}\sqrt{\eta_c\kappa_6} - \frac{\kappa_6}{2}\langle\hat{a}_6\rangle,\tag{2c}$$

$$\frac{\mathrm{d}\langle\hat{q}_i^2\rangle}{\mathrm{d}t}=\frac{1}{m_i}\langle\hat{p}_i\hat{q}_i+\hat{q}_i\hat{p}_i\rangle,\quad i=1,2,\cdots,6, \tag{2d}$$

$$\frac{\mathrm{d}\langle\hat{p}_i\hat{q}_i+\hat{q}_i\hat{p}_i\rangle}{\mathrm{d}t}=\frac{2}{m_i}\langle\hat{p}_i^2\rangle-2m_i\omega_{mi}^2\langle\hat{q}_i^2\rangle-4\hbar g_i\langle\hat{q}_i^2\rangle\langle\hat{a}_i^+\rangle\langle\hat{a}_i\rangle-\gamma_{mi}\langle\hat{p}_i\hat{q}_i+\hat{q}_i\hat{p}_i\rangle,\quad i=1,2,\cdots,6, \tag{2e}$$

$$\frac{\mathrm{d}\langle\hat{p}_i^2\rangle}{\mathrm{d}t}=-(m_i\omega_{mi}^2+2\hbar g_i\langle\hat{a}_i^+\rangle\langle\hat{a}_i\rangle)\langle\hat{p}_i\hat{q}_i+\hat{q}_i\hat{p}_i\rangle-2\gamma_{mi}\langle\hat{p}_i^2\rangle+(1+2\overline{n})\gamma_{mi}\hbar m_i\omega_{mi},\quad i=1,2,\cdots,6, \tag{2f}$$

In Eq. (2f), the final term results from the coupling of the mirrors to the thermal environment, where $\overline{n}=(\mathrm{e}^{\frac{\hbar\omega_{mi}}{K_BT}}-1)^{-1}$ is the mean thermal phonon occupation number of energy $\hbar\omega_{mi}$ at environmental temperature T, k_B is Boltzmann's constant [3], and γ_{mi} is the damping rate of mirror i. The terms describing the input vacuum noise for the cavities and the Langevin force for the mirrors disappear thank to their zero mean values.

Next, under the condition that the probe field is much weaker than the coupling field, we can acquire the steady-state results of Eq. (2) by making the ansatz

$$\langle\hat{o}\rangle=o_s+o_+\mathrm{e}^{-\mathrm{i}\delta t}+o_-\mathrm{e}^{\mathrm{i}\delta t}, \tag{3}$$

where $\hat{o}$ denotes any one of these quantities $\hat{a}_i$, $\hat{p}_i^2$, $\hat{q}_i^2$, $\hat{q}_i\hat{p}_i+\hat{p}_i\hat{q}_i$ $(i=1,2,\cdots,6)$. Eq. (3) contains three components with frequencies ω_{ci},ω_p and $2\omega_{ci}-\omega_p$, which are marked by the subscripts "s", "+" and "−", respectively. Upon substituting Eq. (3) into Eq. (2) and ignoring terms that contains the product of more than one small quantity, we obtained an expression for a_{1+} through a series of computations, see Appendix A for the six-cavity situation. The above calculation process is often used to study the OMSs, but now we can use the OMPY program to perform this calculation and thereby obtain a numerical result for a_{1+} directly. Oscillating at the probe frequency ω_p, the component of the output field is given as $\varepsilon_{out}=\sqrt{\eta_c\kappa_1}a_{1+}/\varepsilon_p$, and the probe absorption property of the system is described by the real part of the output field, namely $\varepsilon_R=\mathrm{Re}[\varepsilon_{out+}]$.

3 Absorption properties of multiple-cavity chain

In this section, we focus on the absorption properties of a cavity chain of given length in which only one cavity exhibits an optomechanical interaction.

In order to numerically analyze the absorption properties of the probe field in a quadratically coupled OMS, we use the following parameters [3, 17]: an environment temperature $T=90$ K, a wavelength of the coupling field of $\lambda_i=\frac{2\pi c}{\omega_{ci}}=532$ nm, a cavity length of $L=L_i=6.7$ cm, a cavity delaying rate of $\kappa=\kappa_i=4\pi\times10^4$ Hz, a mirror mass of $m_i=10^{-9}$ g, a mirror frequency of $\omega_m=\omega_{mi}=2\pi\times10^5$ Hz, a mirror damping rate of $\gamma=\gamma_{mi}=20\ \mathrm{s}^{-1}$, a mirror reflectivity of $R=0.45$, and hence a quadratic coupling constant of $g_i=\frac{8\pi^2c}{\lambda_i^2L}\sqrt{\frac{R}{1-R}}=2\pi\times1.8\times10^{23}$ Hz·m^{-2}. The following discussion pertains to two-phonon resonance, that is, $\Delta_i'=\Delta_{ci}+g_iQ_{is}=2\omega_{mi}$, where Q_{is} are the steady-state solutions of $\hat{q}_i^2$, and the detuning between the first coupling and the probe field is redefined by $\sigma=\delta-2\omega_m$ to display the probe transparency properties around the two-phonon resonance, where i represents cavity i.

First, we investigate the output spectrum of cavity chain comprising of two cavities, that is, the tunnel coupling between the first and the second cavities is switched on $(J_{1,2}=2\kappa)$, whereas the others are switched off. In Fig. 2, the red solid curve represents the optomechanical interaction in the first cavity, and the blue dashed curve represents the optomechanical interaction in the second cavity. In this case, due to the fact that the tunnel coupling between the first and the second cavities is in the strong regime, i.e., $J\geqslant\kappa$, the two degenerate cavity modes are hybridized and split into two normal modes, as shown in the inset of Fig. 2. This figure shows that the optomechanical interaction in the first cavity induces a transparency window; however, when the optomechanical interaction is switched on only in the second cavity, an absorption peak emerges in the absorption spectrum of the probe field. This effect is similar to the linear coupling

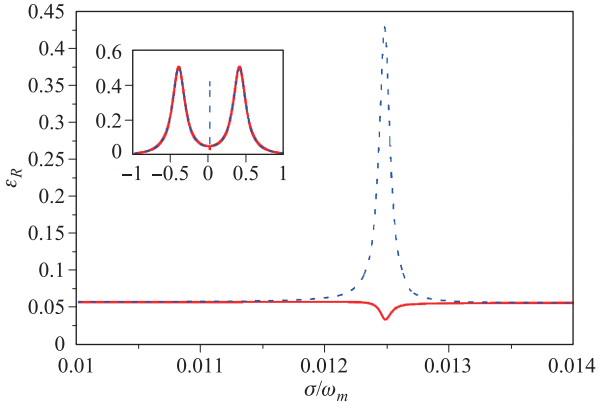

Fig. 2 Absorption of the output field ε_R as a function of the normalized frequency σ/ω_m. Here, cavity chain is composed of two cavity, i.e., only switch on the tunnel coupling between the first two cavities $(J_{1,2}=2\kappa)$. The red solid curve shows that the first cavity is optomechanical cavity while the second cavity is bare optical cavity ($P_1=180$ μW, $g_1=2\pi\times1.8\times10^{23}$ Hz·m^{-2}, $P_2=0, g_2=0$); the blue dashed curve shows that the second cavity is optomechanical cavity and the first cavity is bare optical cavity ($P_1=0, g_1=0, P_2=180$ μW, $g_2=2\pi\times1.8\times10^{23}$ Hz·m^{-2}).

case [27]. In addition, we found that the positions of the peak and the dip are very close.

Next, we switched on the photonic coupling of the first six cavities [$J_{i,i+1} = 2\kappa$ $(i = 1, 2, \cdots, 5)$] and considered how the position of the optomechanical cavity influences the output spectrum of this system. In Fig. 3, the optomechanical interaction is in different cavities, namely, the first cavity (Fig. (3a), red solid curve), the sixth cavity (Fig. 3(b), red solid curve), the second cavity [Fig. 3(b), green dash-dotted curve], the fifth cavity [Fig. 3(a), green dash-dotted curve], the third cavity [Fig. 3(a), blue dashed curve], the fourth cavity [Fig. 3(b), blue dashed curve]. From the inset of Fig. 3, we also found that the six cavity modes split into six normal modes. Figure 3(a) shows that an OMIT occurs when the optomechanical interaction is at an odd-numbered location in the cavity chain. As shown in Fig. 3(a), with the transparency dip becoming shallower the farther the optomechanical cavity is from the probe cavity. Figure 3(b) shows that optomechanically induced absorption (OMIA) emerges in the absorption spectrum of the probe field when the optomechanical interaction is in an even-numbered cavity and similar to Fig. 3(a), the absorption peak becomes shallower when the optomechanical cavity keeps moving away from the probe cavity. In addition, the red solid curves in Figs. 3(a) and (b) show that the positions of the OMIT dip and the OMIA peak are almost the same, which is caused by the symmetry of the system structure. When the optomechanical interaction is in the second or fifth cavity and in the third or fourth cavity, the conclusions are the same.

Finally, we expanded the cavity chain from six cavities to fifteen cavities, that is, $J_{1,2} = J_{2,3} = \cdots = J_{i,i+1} = 2\kappa$ $(i = 1, 2, \cdots, 14)$, as shown in Fig. 4. In this case, the probe field is at the first cavity, and the output spectrum depends on the position of the optomechanical cavity. Figure 4 contains two graphs, namely, (a) the value ε_R of the OMIT dip or OMIA peak in the absorption spectrum and (b) the position of the dip or peak σ/ω_m as a function of the position N of the optomechanical cavity. In Fig. 4(a), the blue dashed curve shows the value of the dip of the transparency window when the optomechanical cavity is at an odd-numbered position, and the green dash-dotted curve shows the absorption peak induced by optomechanical interaction when the optomechanical cavity is at an even-numbered position. These two curves show that as the distance between the probe cavity and the optomechanical cavities increased, the minimum value of the OMIT dip and the maximum value of the OMIA peak trend to the same value when the cavity number is beyond 15. This means that the effect of optomechanical interaction weakens gradually as the optomechanical cavity becomes farther from the probe cavity. Figure 4(b) shows the position of the transparency dip or absorption peak generated by the optomechanical interaction, from which we found that this position depends partly on the structure of the cavity chain: when two optomechanical cavities are at symmetric positions in the chain, the positions of the dip and the peak are almost the same.

Thus, by combining panels (a) and panels (b) in Fig. 3 and Fig. 4, we can identify the position of the optomechanical interaction: first the optomechanical interaction is at either an odd- or even-numbered position depending on whether there is an OMIT or an OMIA, respectively, in the output field; then, by combining with the value of the transparency dip or absorption peak, the exact position of the optomechanical interaction can be obtained.

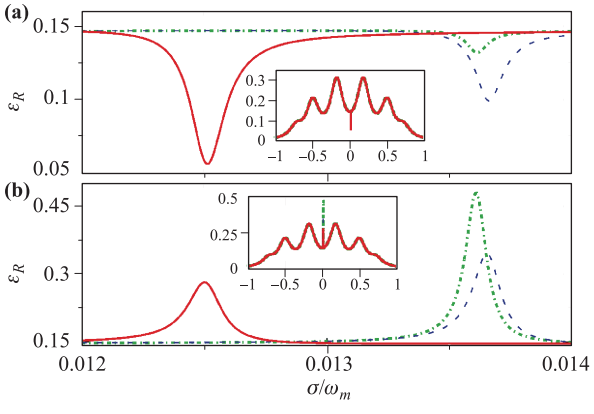

Fig. 3 Absorption of the output field ε_R as a function of the normalized frequency σ/ω_m. Here, cavity chain is composed of six cavities, i.e., switch on the tunnel coupling between the first six cavities [$J_{i,i+1} = 2\kappa$ $(i = 1, 2, \cdots, 5)$]. In panel **(a)**, the optomechanical cavity is chosen to be in the first, third, fifth cavity; while in panel **(b)**, the optomechanical cavity is chosen to be in the sixth, fourth, second cavity, which is shown in the red solid, blue dashed, and green dashed-dot curves, respectively.

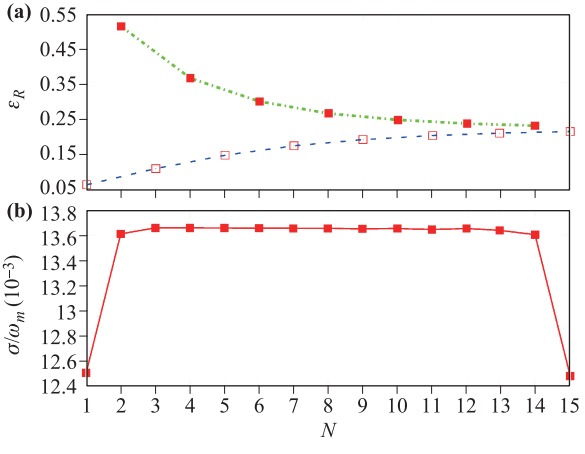

Fig. 4 Cavity chain is composed of 15 cavities, and the probe field is at the first cavity. In panel **(a)**, the value of the absorption dip or peak induced by optomechanical interaction as a function of the position of the optomechanical cavity: the position of the optomechanical cavity is odd or even shown in blue dashed or green dashed-dotted curve, respectively. In panel **(b)**, the red solid curve shows that the normalized frequency σ/ω_m corresponding to the absorption dip or peak changes over the position of the optomechanical cavity.

4 Absorption properties of infinite-cavity chain

In the previous section, we considered how the absorption properties in a cavity chain with a given length vary with the position of the optomechanical interaction. Now, we investigate how increasing the number of bare cavities following the optomechanical cavity affects the probe absorption properties. In this section, we discuss the cavity-chain system in two aspects, namely, (i) increasing the number of bare cavities after the optomechanical cavity and (ii) increasing the number of bare cavities on the both sides of the optomechanical cavity, which we can think of as an infinite-cavity chain.

We begin by considering the situation in which the optomechanical interaction is in the first cavity of the chain and always induces a transparency window in the absorption spectrum. Figure 5 contains two graphs, namely, (a) the value ε_R of the OMIT dip in the absorption spectrum and (b) the position of the dip σ/ω_m as a function of the number N of bare optical cavities. Figure 5(a) shows that the value of the dip tends to be fixed as the number N of bare cavities is increased; the value of the dip increases for odd N and decreases for even N as N is increased. Figure 5(b) shows the position of the dip which exhibits a fluctuation that weakens gradually as N is increased.

Next, we investigate how the absorption properties vary with the number of bare cavities when the optomechanical interaction is in the second cavity and always induces an absorption peak in the output field. Figure 6(a) shows the value of the absorption peak as a function of the number (N) of bare optical cavities. Again, we found that the value of the peak tends to be fixed as N is increased: the value of the peak decreases for odd N and increased for even N. Figure 6(b) shows that the position of the absorption peak changes with N. By comparing Fig. 5(b) and Fig. 6(b), we observed that the position exhibits the same tendency in both cases.

Then, we focus on the case in which we increase the number (N) of bare cavities on both sides of the optomechanical cavity, and we investigate further how N affects the output field. Here, the optomechanical interaction and the probe field are in the middle cavity. As N is increased, we observe that the optomechanical interaction always induces a transparency window in the absorption spectrum. Figure 7 shows the value ε_R of the transparency dip in the absorption spectrum and the position σ/ω_m of the dip as a function N. Figure 7(a) shows ε_R increases with N when N is odd (blue dashed cureve) but decreases with N when N is even (green dash-dotted cureve); however, these two curves ultimately tend to a fixed value. In Fig. 7(b), except for $N = 1$, the other positions of the dip simply fluctuate around a fixed value, with the fluctuation amplitude decreasing gradually with N.

Figures 5–7 show that as the number of cavities is increased, the values of the transparency dip and absorption peak tend to become steady, as do their positions. This means that the influence of the optomechanical interaction on the output field weakens as the number of cavities is increased, which is very important for choosing the length of the cavity chain.

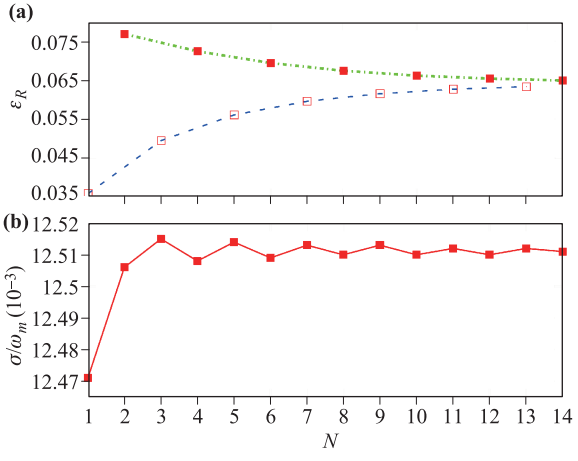

Fig. 5 The length of the cavity chain is changeable by increasing bare cavities behind the optomechanical cavity, and both the optomechanical cavity and the probe field are at the first cavity. In panel **(a)**, the value of the optomechanical transparency dip as a function of the number N of bare optical cavities behind the optomechanical cavity, the number is odd or even shown in blue dashed or green dashed-dotted curve, respectively; in panel **(b)**, the red solid curve shows that the normalized frequency σ/ω_m, which the transparency dip corresponds to, changes over the number of bare optical cavities.

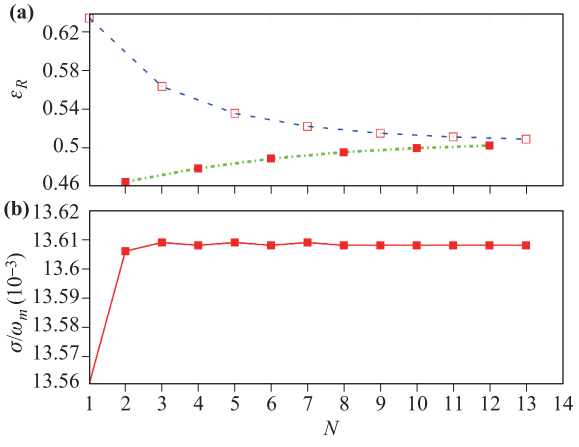

Fig. 6 The length of cavity chain is changeable by increasing bare cavities behind the optomechanical cavity, and the optomechanical cavity is at the second cavity while the probe field is at the first cavity. In panel **(a)**, the value of the optomechanical absorption peak as a function of the number N of bare optical cavities after the optomechanical cavity, the number is odd or even shown in blue dashed or green dashed-dotted curve, respectively; in panel **(b)**, the red solid curve shows that the normalized frequency σ/ω_m, which the absorption peak corresponds to, changes over the number of bare optical cavities.

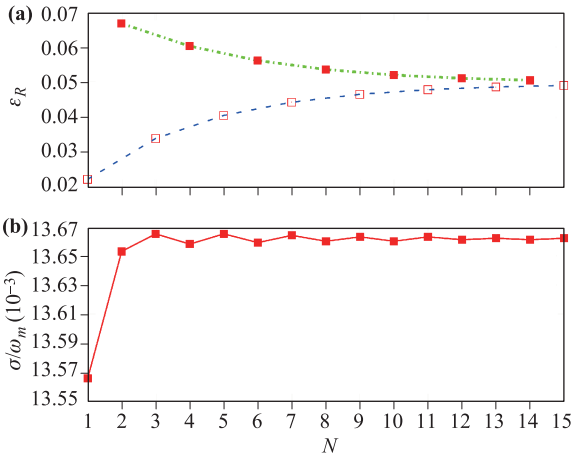

Fig. 7 The length of the cavity chain is changeable by increasing bare cavities on both side of the optomechanical cavity, and both the optomechanical interaction and the probe field are at the middle cavity. In panel **(a)**, the value of the optomechanical transparency dip as a function of the number N of bare optical cavities in one side of the optomechanical cavity, the number is odd or even shown in blue dashed or green dashed-dotted curve, respectively; in panel **(b)**, the red solid curve shows that the normalized frequency σ/ω_m, corresponding to the transparency dip, changes over the number of bare optical cavity.

5 Summary

In conclusion, we have investigated how the structure of a cavity chain influences the spectral properties of the probe output field, and we found that such a system exhibits an OMIT and an OMIA caused by the optomechanical interactions. In order to manifest the main effects of the optomechanical interaction, the cavity chain is confined to the degenerate situation. Probing the first cavity in a chain of given length, the position of the optomechanical interaction determines whether a transparency window or an absorption peak appears in the output field and when the optomechanical interaction is far from the probe field, the value of the transparency window or absorption peak decreases. These can be used in turn to determine the position of the optomechanical interaction. Moreover, when we increase the number of bare cavities either after or on either side of the optomechanical cavity, the OMIT and OMIA do not change qualitatively. These show that the OMIT and OMIA are determined by the position of the optomechanical interaction relative to the probe field. However, the extreme value of OMIT or OMIA decay asymptotically with the number of the bare cavities, which implies a limitation for the length of the chain. These interesting phenomena should be of much importance for quantum information processing by optomechanical cavity chains. In addition, the delicate tunability can be realized in not only one dimensional but also higher dimensional optomechanical crystal, which can also be treated by OMPY.

Acknowledgements This work was supported by the NSFC (Grant No. 11874273), the Project of Heibei Educational Department, China (No. ZD2018015), and the Key Project of Sichuan Science and Technology Program (No. 2019YFSY0044).

Appendix A

Due to the assumption that the coupling field is stronger than the probe field, the variables of the movable mirror and cavity fields are divided into the steady parks and the fluctuation ones: $\hat{O} = O_s + \delta\hat{O}$, where $\hat{O}$ denotes the varables: $\hat{a}_i$, $\hat{p}_i^2$, $\hat{q}_i^2$, $\hat{p}_i\hat{q}_i + \hat{q}_i\hat{p}_i$ $(i = 1, 2, \cdots 6)$. The steady parts of the variables are given by

$$a_{1s} = \frac{-\mathrm{i}J_{1,2}C_2 + \varepsilon_{c1}\sqrt{\eta_c\kappa_1}}{\mathrm{i}\Delta_1' + \frac{\kappa_1}{2} + \frac{J_{1,2}^2}{D_2}}, \tag{A1}$$

$$a_{is} = \frac{-\mathrm{i}J_{i-1,i}a_{i-1s} - \mathrm{i}J_{i,i+1}C_{i+1} + \varepsilon_{ci}\sqrt{\eta_c\kappa_i}}{D_i}, \quad i = 2, \cdots, 5, \tag{A2}$$

$$a_{6s} = \frac{-\mathrm{i}J_{5,6}a_{5s} + \varepsilon_{c6}\sqrt{\eta_c\kappa_6}}{\mathrm{i}\Delta_6' + \frac{\kappa_6}{2}}, \tag{A3}$$

$$p_{is}^2 = \frac{1 + 2\overline{n}}{2}\hbar m_i\omega_{mi}, \quad i = 1, 2, \cdots, 6, \tag{A4}$$

$$p_{is}q_{is} + q_{is}p_{is} = 0, \quad i = 1, 2, \cdots, 6, \tag{A5}$$

$$q_{is}^2 = \frac{p_{is}^2}{m_i^2\omega_{mi}^2 + 2\hbar m_i g_i a_{is}^* a_{is}}, \quad i = 1, 2, \cdots, 6, \tag{A6}$$

where

$$D_6 = \mathrm{i}\Delta_6' + \kappa_6/2, \tag{A7}$$

$$C_6 = \frac{\varepsilon_{c6}\sqrt{\eta_c\kappa_6}}{D_6}, \tag{A8}$$

$$D_i = \mathrm{i}\Delta_i' + \kappa_i/2 + \frac{J_{i,i+1}^2}{D_{i+1}}, \quad i = 2, \cdots, 5, \tag{A9}$$

$$C_i = \frac{\varepsilon_{ci}\sqrt{\eta_c\kappa_i} - iJ_{i,i+1}C_{i+1}}{D_i}, \quad i = 2, \cdots, 5. \tag{A10}$$

The dynamical behaviors of the system can be obtained by solving the equation of the motion for the fluctuations:

$$\frac{\mathrm{d}\langle\delta\hat{a}_1\rangle}{\mathrm{d}t} = -(\kappa_1/2 + \mathrm{i}\Delta_1')\langle\delta\hat{a}_1\rangle - \mathrm{i}g_1a_{1s}\langle\delta\hat{q}_1^2\rangle - \mathrm{i}J_{1,2}\langle\delta\hat{a}_2\rangle + \varepsilon_p\sqrt{\eta_c\kappa_1}\mathrm{e}^{-\mathrm{i}\delta t}, \tag{A11a}$$

$$\frac{\mathrm{d}\langle\delta\hat{a}_i\rangle}{\mathrm{d}t} = -(\kappa_i/2 + \mathrm{i}\Delta_i')\langle\delta\hat{a}_i\rangle - \mathrm{i}g_ia_{is}\langle\delta\hat{q}_i^2\rangle - \mathrm{i}J_{i-1,i}\langle\delta\hat{a}_{i-1}\rangle - \mathrm{i}J_{i,i+1}\langle\delta\hat{a}_{i+1}\rangle, \quad i = 2, \cdots, 5, \tag{A11b}$$

$$\frac{\mathrm{d}\langle\delta\hat{a}_6\rangle}{\mathrm{d}t} = -(\kappa_6/2 + \mathrm{i}\Delta_6')\langle\delta\hat{a}_6\rangle - \mathrm{i}g_6 a_{6s}\langle\delta\hat{q}_6^2\rangle - \mathrm{i}J_{5,6}\langle\hat{a}_5\rangle, \tag{A11c}$$

$$\frac{\mathrm{d}\langle\delta\hat{q}_i^2\rangle}{\mathrm{d}t} = \frac{1}{m_i}\langle\delta(\hat{p}_i\hat{q}_i + \hat{q}_i\hat{p}_i)\rangle, \quad i = 1, 2, \cdots, 6, \tag{A11d}$$

$$\begin{aligned}\frac{\mathrm{d}\langle\delta(\hat{p}_i\hat{q}_i + \hat{q}_i\hat{p}_i)\rangle}{\mathrm{d}t} = {} & \frac{2}{m_i}\langle\delta\hat{p}_i^2\rangle - 2m_i\omega_{mi}^2\langle\delta\hat{q}_i^2\rangle - 4\hbar\{g_i a_{is}^* a_{is}\langle\delta\hat{q}_i^2\rangle \\ & + q_{is}^2[g_i a_{is}^*\langle\delta\hat{a}_i\rangle + g_i a_{is}\langle\delta\hat{a}_i^+\rangle]\} - \gamma_{mi}\langle\delta(\hat{p}_i\hat{q}_i + \hat{q}_i\hat{p}_i)\rangle, \quad i = 1, 2, \cdots, 6,\end{aligned} \tag{A11e}$$

$$\frac{\mathrm{d}\langle\delta\hat{p}_i^2\rangle}{\mathrm{d}t} = -(m_i\omega_{mi}^2 + 2\hbar g_i a_{is}^* a_{is})\langle\delta(\hat{p}_i\hat{q}_i + \hat{q}_i\hat{p}_i)\rangle - 2\gamma_{mi}\langle\delta\hat{p}_i^2\rangle, \quad i = 1, 2, \cdots, 6, \tag{A11f}$$

where $\Delta_i' = \Delta_{ci} + g_i q_{is}^2$ $(i = 1, 2, \cdots, 6)$ are the effective detunings.

References and notes

1. M. Aspelmeyer, T. J. Kippenberg, and F. Marquardt, Cavity optomechanics, *Rev. Mod. Phys.* 86(4), 1391 (2014)
2. J. Q. Liao and C. K. Law, Cooling of a mirror in cavity optomechanics with a chirped pulse, *Phys. Rev. A* 84(5), 053838 (2011)
3. S. Huang and G. S. Agarwal, Electromagnetically induced transparency from two-phonon processes in quadratically coupled membranes, *Phys. Rev. A* 83(2), 023823 (2011)
4. M. Aspelmeyer, P. Meystre, and K. Schwab, Quantum optomechanics, *Phys. Today* 65(7), 29 (2012)
5. J. Teufel, T. Donner, D. Li, J. Harlow, M. Allman, K. Cicak, A. Sirois, J. Whittaker, K. Lehnert, and R. Simmonds, Sideband cooling of micromechanical motion to the quantum ground state, *Nature* 475(7356), 359 (2011)
6. S. Machnes, J. Cerrillo, M. Aspelmeyer, W. Wieczorek, M. B. Plenio, and A. Retzker, Pulsed laser cooling for cavity optomechanical resonators, *Phys. Rev. Lett.* 108(15), 153601 (2012)
7. J. Chan, T. P. M. Alegre, A. H. Safavi Naeini, J. T. Hill, A. Krause, S. Groblacher, M. Aspelmeyer, and O. Painter, Laser cooling of a nanomechanical oscillator into its quantum ground state, *Nature* 478(7367), 89 (2011)
8. M. Bhattacharya and P. Meystre, Trapping and cooling a mirror to its quantum mechanical ground state, *Phys. Rev. Lett.* 99(7), 073601 (2007)
9. P. Rabl, Photon blockade effect in optomechanical systems, *Phys. Rev. Lett.* 107(6), 063601 (2011)
10. M. Ludwig, A. H. Safavi-Naeini, O. Painter, and F. Marquardt, Enhanced quantum nonlinearities in a two-mode optomechanical system, *Phys. Rev. Lett.* 109(6), 063601 (2012)
11. X. Y. Lü, W. M. Zhang, S. Ashhab, Y. Wu, and F. Nori, Quantum-criticality-induced strong Kerr nonlinearities in optomechanical systems, *Sci. Rep.* 3(1), 2943 (2013)
12. Y. W. Hu, Y. F. Xiao, Y. C. Liu, and Q. H. Gong, Optomechanical sensing with on-chip microcavities, *Front. Phys.* 8(5), 475 (2013)
13. S. Mancini, V. Giovannetti, D. Vitali, and P. Tombesi, Entangling macroscopic oscillators exploiting radiation pressure, *Phys. Rev. Lett.* 88(12), 120401 (2002)
14. M. J. Hartmann and M. B. Plenio, Steady state entanglement in the mechanical vibrations of two dielectric membranes, *Phys. Rev. Lett.* 101(20), 200503 (2008)
15. D. Vitali, S. Gigan, A. Ferreira, H. R. Bohm, P. Tombesi, A. Guerreiro, V. Vedral, A. Zeilinger, and M. Aspelmeyer, Optomechanical entanglement between a movable mirror and a cavity field, *Phys. Rev. Lett.* 98(3), 030405 (2007)
16. J. Q. Liao and L. Tian, Macroscopic quantum superposition in cavity optomechanics, *Phys. Rev. Lett.* 116(16), 163602 (2016)
17. X. G. Zhan, L. G. Si, A. S. Zheng, and X. Yang, Tunable slow light in a quadratically coupled optomechanical system, *J. Phys. At. Mol. Opt. Phys.* 46(2), 025501 (2013)
18. A. H. Safavi-Naeini, T. P. M. Alegre, J. Chan, M. Eichenfield, M. Winger, Q. Lin, J. T. Hill, D. E. Chang, and O. Painter, Electromagnetically induced transparency and slow light with optomechanics, *Nature* 472(7341), 69 (2011)
19. K. Stannigel, P. Komar, S. J. M. Habraken, S. D. Bennett, M. D. Lukin, P. Zoller, and P. Rabl, Optomechanical quantum information processing with photons and phonons, *Phys. Rev. Lett.* 109(1), 013603 (2012)
20. A. Safavi-Naeini and O. Painter, Proposal for an optomechanical traveling wave phonon–photon translator, *New J. Phys.* 13(1), 013017 (2011)
21. M. Schmidt, M. Ludwig, and F. Marquardt, Optomechanical circuits for nanomechanical continuous variable quantum state processing, *New J. Phys.* 14(12), 125005 (2012)
22. M. Pang, W. He, X. Jiang, and P. Russell, All-optical bit storage in a fibre laser by optomechanically bound states of solitons, *Nat. Photonics* 10(7), 454 (2016)
23. S. Forstner, S. Prams, J. Knittel, E. D. van Ooijen, J. D. Swaim, G. I. Harris, A. Szorkovszky, W. P. Bowen, and H. Rubinsztein-Dunlop, Cavity optomechanical magnetometer, *Phys. Rev. Lett.* 108(12), 120801 (2012)
24. M. Li, W. Pernice, and H. X. Tang, Ultrahigh-frequency nano-optomechanical resonators in slot waveguide ring cavities, *Appl. Phys. Lett.* 97(18), 183110 (2010)

25. C. Jiang, H. Liu, Y. Cui, X. Li, G. Chen, and B. Chen, Electromagnetically induced transparency and slow light in two-mode optomechanics, *Opt. Express* 21(10), 12165 (2013)

26. K. H. Qu and G. S. Agarwal, Phonon-mediated electromagnetically induced absorption in hybrid opto-electromechanical systems, *Phys. Rev. A* 87, 031802(R) (2013)

27. B. P. Hou, L. F. Wei, and S. J. Wang, Optomechanically induced transparency and absorption in hybridized optomechanical systems, *Phys. Rev. A* 92(3), 033829 (2015)

28. Z. Qian, M. M. Zhao, B. P. Hou, and Y. H. Zhao, Tunable double optomechanically induced transparency in photonically and phononically coupled optomechanical systems, *Opt. Express* 25(26), 33097 (2017)

29. A. B. Shkarin, N. E. Flowers-Jacobs, S. W. Hoch, A. D. Kashkanova, C. Deutsch, J. Reichel, and J. G. E. Harris, Optically mediated hybridization between two mechanical modes, *Phys. Rev. Lett.* 112(1), 013602 (2014)

30. C. Bai, B. P. Hou, D. G. Lai, and D. Wu, Tunable optomechanically induced transparency in double quadratically coupled optomechanical cavities within a common reservoir, *Phys. Rev. A* 93(4), 043804 (2016)

31. A. Tomadin, S. Diehl, M. D. Lukin, P. Rabl, and P. Zoller, Reservoir engineering and dynamical phase transitions in optomechanical arrays, *Phys. Rev. A* 86(3), 033821 (2012)

32. W. Chen and A. A. Clerk, Photon propagation in a one-dimensional optomechanical lattice, *Phys. Rev. A* 89(3), 033854 (2014)

33. G. D. de Moraes Neto, F. M. Andrade, V. Montenegro, and S. Bose, Quantum state transfer in optomechanical arrays, *Phys. Rev. A* 93(6), 062339 (2016)

34. Z. Duan and B. Fan, Coherently slowing light with a coupled optomechanical crystal array, *Europhys. Lett.* 99(4), 44005 (2012)

35. OMPY is programmed by python combined with fortran, devoted to solve an optomechanical system consisted of multiple cavities by the standard linearization method. OMPY starts with an optomechanical Hamiltonian and then generates the Heisenberg–Langevin equations, which are solved by the standard linearization procedure, automatically.